Nitrogen-doped activated carbon derived from biomass waste for effective removal of doxycycline from aqueous solution: characterization and adsorption mechanism

Qingyun Li[1] · Ningjie Liang[1] · Weihua Zou[1] · Xiuli Han[1,2] · Chun Chang[1,2] · Junying Chen[1,2]

Abstract

The nitrogen-doped activated carbon (NAC) with high specific area ($3140.76 \text{ m}^2 \cdot \text{g}^{-1}$) derived from pomelo peel was prepared using hydrothermal carbonization, nitrogen doping and KOH activation method for the effective removal of Doxycycline (DOX) from aqueous solution. NAC showed exceptional adsorption efficacy for DOX than non-doped activated carbon (AC), which was attributed to the rich N-containing functional groups on the NAC surface and well-developed pore structure. The adsorption equilibrium data of DOX on NAC was fitted well to the Sips isotherm model and the adsorption process was spontaneous, endothermic and randomness-increasing. The Elovich kinetic model could better describe the adsorption process of DOX. The adsorption mechanisms of DOX onto NAC could be attributed to the hydrogen bonding, π-π electron donor-acceptor (EDA) interaction, hydrophobic effect and electrostatic interaction. Besides, the N-doping enhanced the adsorption performance of NAC. The maximum saturated adsorption capacity of NAC was $1559.35 \text{ mg} \cdot \text{g}^{-1}$ at 298 K, indicating that the NAC could be a promising adsorbent for removing Doxycycline from wastewater.

Keywords Nitrogen-doped activated carbon · High specific·surface area · Doxycycline · Adsorption · Pomelo peel

1 Introduction

Antibiotics are commonly used in human disease therapy and livestock breeding for antibacterial and bactericidal purpose [1]. A large amount of wastewater was generated in the process of production and practical application of antibiotics, resulting in the problem of water pollution, which had garnered significant attention from the international scientific community [2]. Chemical property of these released antibiotics would make them hard to degrade and decomposed. Eventually, they may continuously accumulate in the human body along the food chain [3]. Especially in recent years, the usage of antibiotics witnessed a significant increase due to the outbreak of COVID-19 and other epidemics. Doxycycline hyclate, as a type of tetracycline antibiotics, can be used to treat COVID-19-related diseases [4]. However, these antibiotics cannot be fully absorbed by the human and animals, so that 65–80% of them would be excreted in the external water environment via them metabolism [5]. The residual antibiotics contribute to the release of antibiotic resistance genes (ARGs) into the environment, rendering conventional antibiotic treatments ineffective, making it difficult to control infection-causing bacteria [6]. Moreover, antibiotics presence in aquatic environment, even at trace levels, have been caused harmful impacts on ecological environment and human health. Therefore, these antibiotics are urgent to be efficiently eliminated from wastewater.

At present, several physical, chemical, and biological methods, such as adsorption [7], membrane filtration [8], advanced oxidation processes (AOPs) [9] have been employed to treat antibiotics pollutant. These processes although have been widely used in the field of wastewater treatment, but involve high initial investments, operational costs, and secondary pollution. On the contrary, the adsorption is cost-effective, simple design, convenient operation,

✉ Xiuli Han
  xlhan@zzu.edu.cn

[1] School of Chemical Engineering, Zhengzhou University, Kexue Road 100#, Zhengzhou, Henan 450001, P.R. China

[2] Henan Center for Outstanding Overseas Scientists, Zhengzhou 450001, China

reusable adsorbent and no hazardous by-products [10, 11]. The effectiveness of adsorption is contingent upon the choice of adsorbent materials. Biochar is one of adsorbent materials which has been developed and utilized owing to their abundant material source, low costs, high specific surface area and pore structure [12–14].

In order to improve adsorption characteristic, the biochar adsorbents need to be modified with heteroatom doping method. Chemical modification, an effective mean, is able to elevate the surface chemical activity of biochars [15]. Reportedly, nitrogen doping modified biochar as the promising adsorbent material has received increasing attention [16]. The approaches of nitrogen-doped are mainly divided into post doped and in-situ doped, corresponding to different feedstock sources and treatment processes [17]. The advantage of the post doped approach is that the nitrogen content of the final product can be controlled by adjusting the initial amount of the nitrogen-containing chemicals to meet actual requirement. The relatively high electron affinity of nitrogen atom can promote the adjacent carbon atoms in carbon material to have a higher positive charge density [18]. Moreover, N-containing groups could convert the structure of biochar for interaction with pollutants. These findings revealed that nitrogen-doped activated carbon exhibits excellent electrochemical and adsorption properties [19]. Thus, the experiment in this article focused on comparing the surface functional groups and structural changes before and after nitrogen doping, providing a reasonable explanation for the influence of nitrogen doping on the adsorption process.

In recent years, a variety of raw materials such as cotton stalks, sponge gourd and coconut shells, etc [20–22] have been used in the production of biochar. Pomelo peel is one of the typical agricultural residues. According to the data, an annual output of pomelo is nearly 4.5-5 million tons in China [23]. However, the pomelo peel is often directly discarded as solid residue and not fully utilized. Pomelo peel contains a high carbon content which has great potential for preparing nitrogen-doped activated carbon. In this study, the novel nitrogen-doped activated carbon (NAC) and non-doped activated carbon (AC) derived from pomelo peel were prepared. The activated carbons were characterized by various methods such as SEM, XPS, FTIR, Raman and BET analysis. The adsorption characteristics of Doxycycline hyclate onto the nitrogen-doped activated carbon and non-doped activated carbon were thoroughly investigated to determine the effects of N source addition on its adsorption and the possible adsorption mechanism of Doxycycline on nitrogen-doped activated carbon was also clearly explained.

2 Materials and methods

2.1 Chemicals and reagents

All chemicals were of analytical standard and could be used directly without further purification. The Doxycycline hyclate ($C_{22}H_{24}N_2O_8 \cdot HCl$ 480.89 MW, DOX) was purchased from Macklin Biochemical Co, Ltd. Melamine ($C_3H_6N_6$), KOH, HCl, NaOH, NaCl were obtained from Kermel Co, Ltd. Pomelo peel was provided by a local market in Henan, China.

2.2 Preparation of materials

Pomelo peel was thoroughly cleaned with deionized (DI) water to remove surface impurities and then dried at 358 K. The pomelo peel was crushed to obtain uniform particles for the next step. The preparation method for nitrogen-doped activated carbon involved hydrothermal carbonization, nitrogen doping, and activation process. In this process, 20 g of pomelo peel powder with 200 mL DI water was carbonized in a 250 mL stainless steel autoclave at 493 K for 120 min [20]. The production was filtered, and then dried at 378 K for 480 min to get activated carbon precursor. The activated carbon precursor was mixed with melamine in a mass ratio of 1:1 and then heated in a Muffle furnace at 773 K for 120 min to obtain N-doped sample. The activator KOH and N-doped sample in a mass ratio of 3:1 were activated in a tube furnace at 1023 K for 60 min in N_2 atmosphere [24]. The final product was cool to ambient temperature and washed with DI water until the pH reached neutral, and then dried at 358 K for 720 min. The nitrogen-doped activated carbon was denoted as NAC. The control group activated carbon (AC) was prepared by the above process without the addition of melamine. Figure 1 showed the schematic illustration of the preparation of NAC and AC.

2.3 Characterization of the materials

The specific surface area (SSA) and pore volume were calculated by specific surface area analyzer (BET, JW-BK132F, China) through the N_2 adsorption-desorption method. The morphologies and main elements of materials were determined by scanning electron microscopy (SEM, FEI Quanta 200, U.S.A.) and elementary-analysis (EA, Thermo Scientific Flash 2000, U.S.A.), respectively. Besides, FTIR (Fourier transform spectroscopy) spectrum was obtained by PerkinElmer Spectrum Two (PerkinElmer company, Massachusetts, UK.) to analyze functional groups of NAC and AC. The XPS (X-ray photoelectron spectroscopy) was measured by using AXIS Supra (Shimadzu company, Japan), which was used to recognize the activated carbons' surface

Fig. 1 Schematic illustration of the preparation of NAC and AC

groups of C, N, O and their chemical states. The Raman spectrum was obtained by a Raman spectrometer (Labram HR Evolution, Horiba, France) to analyze the activated carbons' graphitization level.

2.4 pH_{pzc} test of NAC

The point of zero charge (pH_{pzc}) was determined by the salt addition method [25]. 0.02 g of NAC was added into 20 mL NaCl (0.1 mol·L^{-1}) with pH ranging from 3.0 to 10. The pH was adjusted by 0.1 mol·L^{-1} HCl or 0.1 mol·L^{-1} NaOH solution. The final pH was measured after the suspension was shaken at 298 K for 360 min. The value of ΔpH was calculated from the formula:ΔpH = pHinitial- pHfinal. Plot with pHinitial as the x-axis and ΔpH as the y-axis. The pH_{pzc} of NAC was obtained when ΔpH = 0.

2.5 Adsorption tests

The batch adsorption tests were conducted at different concentrations of DOX solution which varied from 50 to 600 mg·L^{-1}. A certain amount of NAC or AC was placed in 100 mL Erlenmeyer flasks with 50 mL of DOX solution. These Erlenmeyer flasks were shaken at 150 rpm in oscillation box at different temperature for 1–720 min. The solution pH was adjusted by 0.1 mol·L^{-1} HCl or 0.1 mol·L^{-1} NaOH solution.

After adsorption, the activated carbons were separated from solution by 0.22 μm membrane. The residual DOX concentrations were measured by ultraviolet spectrophotometry (TU-1080, CN) at a maximum wavelength of 275 nm. The adsorption capacity and removal efficiency were calculated by Eq. (1) and Eq. (2), respectively.

$$q_t = V \frac{(C_0 - C_t)}{m} \tag{1}$$

$$\%R = \frac{(C_0 - C_t)}{C_0} \times 100 \tag{2}$$

q_t (mg·g^{-1}) is adsorption capacity of DOX on NAC or AC at time t, V (L) is the volume of DOX solution, C_0 and C_t (mg·L^{-1}) is initial concentration and concentration at time t of DOX, respectively. m (g) is the mass of NAC or AC.

2.6 Regeneration adsorption experiment

The NAC after the adsorption of DOX was regenerated by immersing in a certain volume of 0.1 mol·L^{-1} NaOH solution at 298 K and the solution was shaken at 150 rpm for 480 min. After that, the NAC was washed several times with DI water until neutral and then dried for the next adsorption process. The NAC was subjected to five adsorption-regeneration cycles.

Fig. 2 N_2 adsorption–desorption isotherms and the pore size distributions of NAC **(a, c)** and AC **(b, d)** before and after DOX adsorption
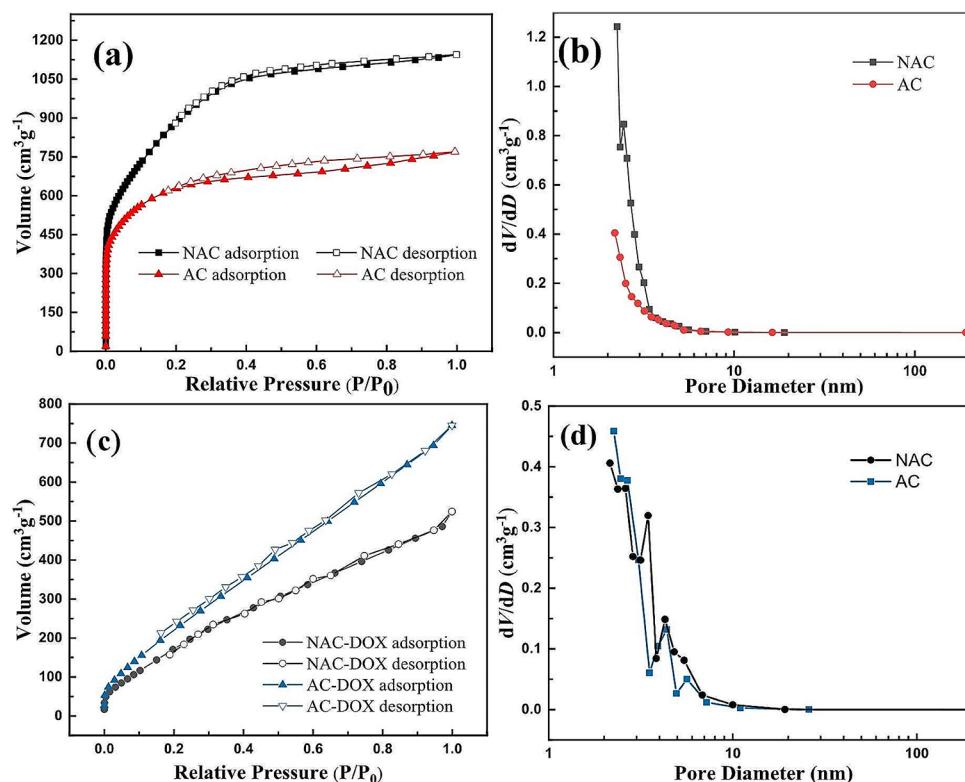
Table 1 Aperture parameters and main elemental content of the NAC and AC

Samples	Surface areas ($m^2 \cdot g^{-1}$)	Pore volume ($cm^3 \cdot g^{-1}$)		Average pore size (nm)	Elemental analysis (wt %)		
		V_{Total}	V_{Mic}		C	H	N
AC	2243.08	1.190	0.817	3.12	71.34	1.85	0.77
NAC	3140.76	1.770	0.781	2.89	75.67	1.14	3.52

# 3 Results and discussion

3.1 Characteristic description

The BET analysis of N_2 adsorption-desorption isotherms and the pore size distributions of NAC and AC before and after DOX adsorption were shown in Fig. 2. These isotherms were type IV adsorption isotherms according to IUPAC classification. The small delayed loops appeared mainly due to capillary condensation, which indicated the presence of micro and mesopores [26, 27]. Table 1 showed aperture parameters and main elemental content of the activated carbons. The SSAs of NAC and AC are 3140.76 $m^2 \cdot g^{-1}$ and 2243.08 $m^2 \cdot g^{-1}$, respectively. The total volume (V_{Tol}) of NAC and AC are 1.770 $cm^3 \cdot g^{-1}$ and 1.190 $cm^3 \cdot g^{-1}$, respectively. It can be speculated that NAC has larger mesopore and macropore volume from V_{Tol} and V_{Mic}. Moreover, the BJH average pore diameter (D_p) are calculated from $D_p=4V_{Tol}/SSA$. The increased SSA and more mesopores of NAC are conducive to provide the more adsorption sites of DOX molecules. However, the specific surface areas of AC

and NAC after adsorption of DOX have decreased to 630.85 $m^2 \cdot g^{-1}$ and 481.99 $m^2 \cdot g^{-1}$ (Fig. 2 (c)), and the pore size distributions have also changed significantly (Fig. 2 (d)). The specific surface area of NAC exhibited a larger decrease than AC after DOX adsorption. This change may be attributed to more DOX molecules adsorbing on the surface or inside of NAC during the adsorption process, which was consistent with the experimental results. These phenomena also illustrated that nitrogen-doped process had greatly changed the surface pores of activated carbon. NAC has a larger of porous structure and provide more sites for DOX molecule diffusion and adsorption than AC.

According to the results of element analysis, the C, H and N contents of NAC are 75.67%, 1.14% and 3.52%, respectively. Compared with AC, the contents of N and C for NAC increased significantly, while the H content decreased. These results indicated that external nitrogen source facilitated to form N-containing functional groups on the surface of NAC.

The morphologies of the pomelo peel after hydrothermal carbonization, AC and NAC were presented in Fig. 3.
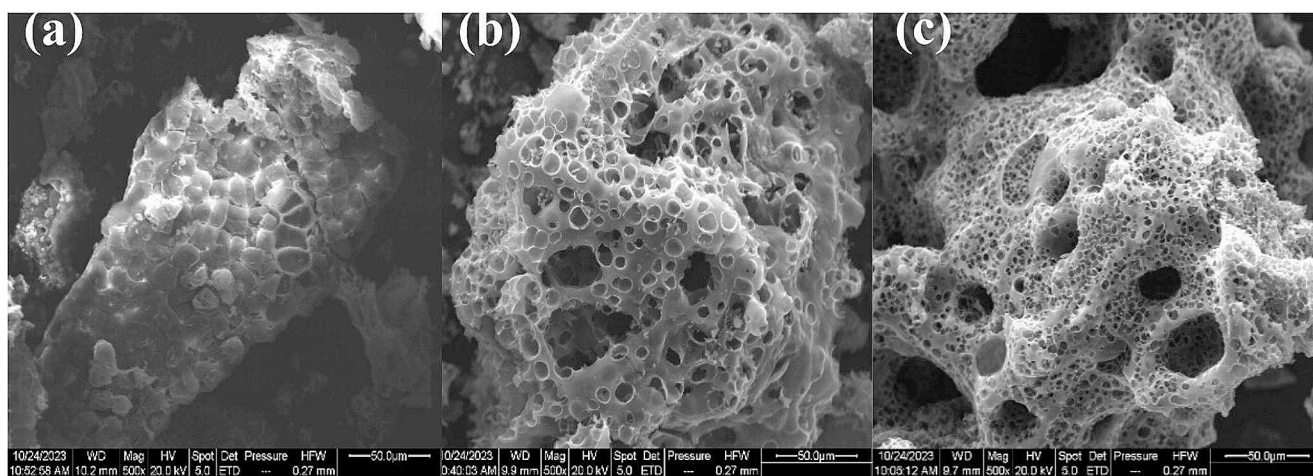
Fig. 3 SEM images of pomelo peel after hydrothermal carbonization **(a)**, AC **(b)** and NAC **(c)**

Figure 3(a) showed that a large number of non-uniform protrusions and few honeycomb-like concavities appeared on pomelo peel after hydrothermal carbonization surface, which was recognized as appearance of the out skin of pomelo peel. From Fig. 3(b), the uneven circle-hollows and deep holes on the AC surface was attributed to the activation of KOH. Besides, Fig. 3(c) showed that NAC had more well-developed honeycombed pores compared with AC. During N-doped process, the gas released by melamine at high temperature was favorable for enhancing pore structures [28]. Theoretically, high capacities of NAC could be partly attributed the fact that more adsorption sites were generated for adsorption of DOX due to more well-developed pores.

The characteristic functional groups of DOX, AC and NAC before and after adsorption of DOX were investigated using FTIR via the KBr pressed pellet method and the result was shown in Fig. 4(a). It was observed that the spectra of AC and NAC were very similar. A comparison between NAC and AC revealed that some peaks showed a slight shift in position and changed in the intensity after the doping of nitrogen. For DOX, the bands at 1676 cm^{-1} and 1460 cm^{-1} were considered as stretching vibration of C=O and C–C of benzene rings, respectively [29, 30]. For NAC, the broad band at 3421 cm^{-1} was –OH vibration and adsorbed water [31]. The band around 2812 cm^{-1} was assigned to aliphatic C-H vibrations [32]. The vibrational characteristic of the C=N was presented at 1630 cm-1 [33]. The signal at 1604 cm-1 was mainly attributed to C=O or in-plane bent vibration of N–H vibration [34]. The small band of 1340 cm^{-1} reflected C-N stretching vibration [24]. For NAC/DOX, the peak of C=O or N-H had a blue shift from 1604 cm^{-1} to 1583 cm^{-1} and the appearance of new peaks at 1676 cm^{-1} and 1460 cm^{-1} after DOX adsorption illustrated that C=O or N-H groups involved in DOX adsorption [35] and the NAC skeleton successfully adsorbed DOX.

Raman spectra (Fig. 4(b)) showed two intense peaks of activated carbons in the wavenumbers around 1350 cm^{-1} and 1580 cm^{-1}, which are commonly recorded as D band (disordered carbon) and G band (graphitic carbon), respectively [36]. The I_D/I_G intensity ratio of NAC is 1.166, which is larger than AC, revealing that the integration of N-atom into the sp^2 carbon network increased more defects of activated carbons [37, 38]. The surface of adsorbents might provide more active sites to promote the adsorption of DOX.

X-ray photoelectron spectroscopy (XPS) has been used to analysis proportion of functional group on the surface of materials. The XPS full spectrums of NAC before and after adsorption of DOX were shown in Fig. 5(a). The content of N element has significantly increased from 2.57 At% to 3.02 At%, indicating that DOX has been successfully embedded in rough surface of NAC. The peaks of NAC and NAC-DOX were fitted by the Avantage software. For the C1s spectra (Fig. 5(b)), the four fitting peaks with the binding energy at 284.82 eV, 286.11 eV, 287.50 eV, and 290.10 eV were confirmed to the C-C, C-O, C=N, and C=O, respectively [39, 40]. There was apparent change from 290.10 eV to 289.76 eV in the peak location of C=O after adsorption as shown in Fig. 5(b), suggesting C=O might be the main contribution to adsorption DOX through hydrogen bonding interaction. Moreover, the peak intensity of C-C and C=N had changed after the adsorption of DOX, which proved the presence of π-π EDA interaction [41].

The N1s spectrum in Fig. 5(d) can be divided into three binding energies at 398.17 eV, 398.79 eV, 400.27 eV, which were consistent with pyridine N, pyrrole N, graphite N, respectively [42]. Melamine could decompose and form N-dopants, i.e., pyridinic N and pyrrole N below the temperature of 873 K [28]. Graphite N has the largest proportion in three nitrogen species of NAC, which could be the π-acceptor because of the strong electronegativity [43].
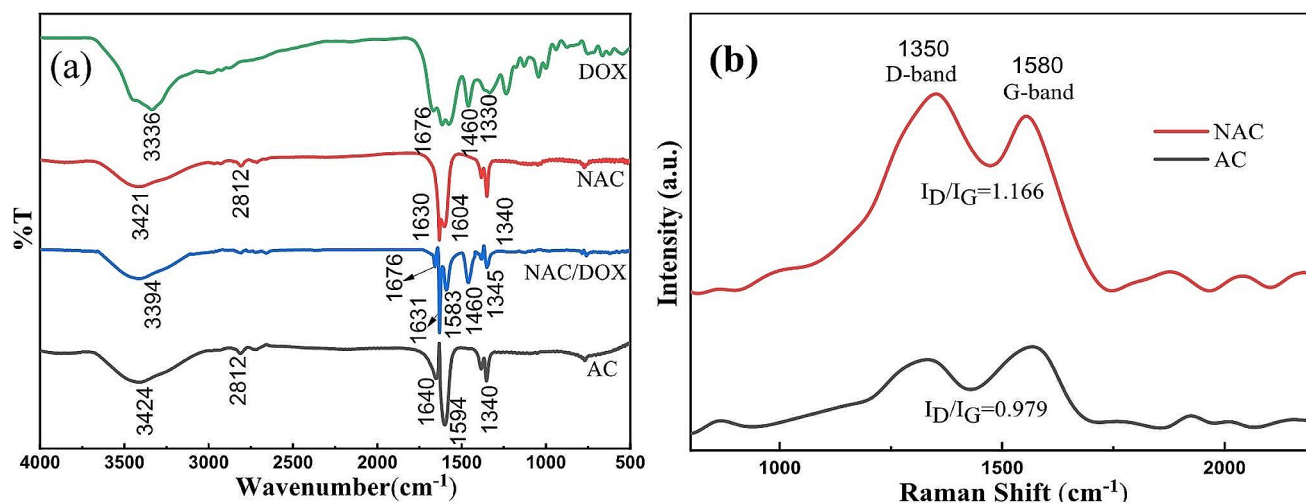
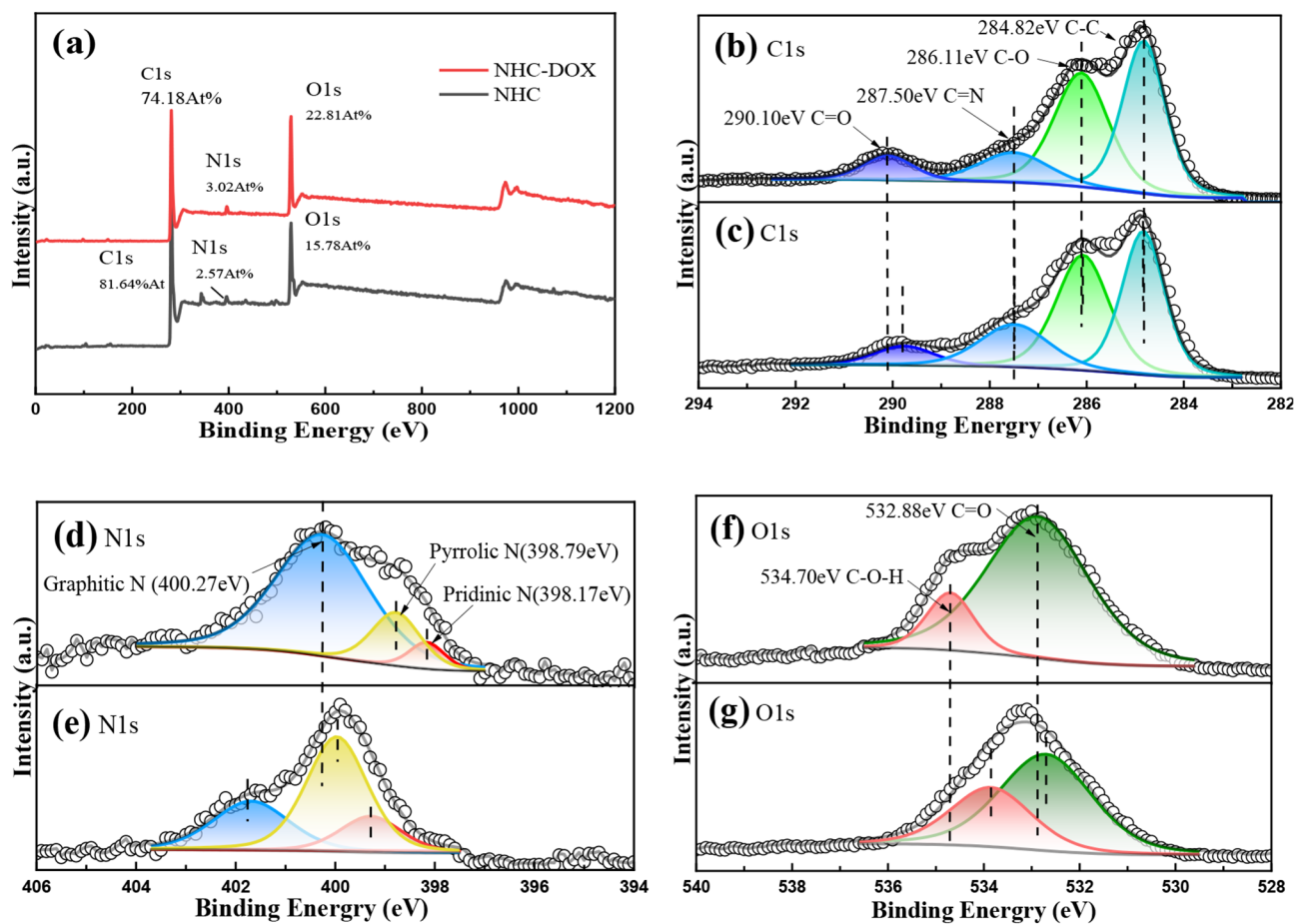**Fig. 4** FT-IR spectra of DOX, NAC, NAC adsorbed DOX, AC **(a)**, and Raman spectra of NAC and AC **(b)**

Fig. 5 XPS survey spectra **(a)**, XPS spectra of C1s **(b, c)**, N1s **(d, e)**, O1s **(f, g)** of NAC before and after adsorption DOX

Pyridine N could further facilitated adsorption performance of activated carbon by hydrophobic effect between DOX and NAC [41]. The binding energies of all nitrogen species in Fig. 4(e) exhibited a shift after the adsorption of DOX, indicating their potential role as adsorption sites during the adsorption process.

As for O1s spectrum shown in Fig. 5(f), 532.88 eV and 534.70 eV were represented for C＝O, C-O-H, respectively [44]. The peaks of C-O-H and C＝O had a shift from 532.88 eV, 534.70 eV of NAC to 532.70 eV and 533.85 eV of NAC after adsorption DOX (Fig. 5(g)), suggesting these groups were concerned with removing DOX. The result was consistent with the FTIR spectrum.

3.2 The effect of time on adsorption of DOX

The contact time is a crucial factor influencing adsorption of DOX on NAC. In the adsorption experiment, the dosage of activated carbons and concentration of DOX solution were 0.2 g·L^{-1} and 200 mg·L^{-1}, respectively. As shown in the Fig. 6(a). DOX was adsorbed rapidly in the first 150 min on both NAC and AC. The adsorption rate of DOX onto AC and NAC slowed down and gradually reached a state of dynamic equilibrium between the DOX desorption and adsorption with time increasing. There was a stronger driving force for mass transfer in the initial adsorption process due to a higher concentration of DOX. With the prolonged time, the adsorption rate becomes slower because more and more adsorption sites on the surface of activated carbons are occupied. The final equilibrium time of NAC and AC were at around 540 min and 480 min, respectively. Finally, 540 min was seen as the adsorption equilibrium time for all other experiments. The equilibrium adsorption capacities of DOX on NAC and AC were 989.55 mg·g^{-1} and 714.52 mg·g^{-1}, respectively, indicating that the N element of NAC also played a role in adsorption process.

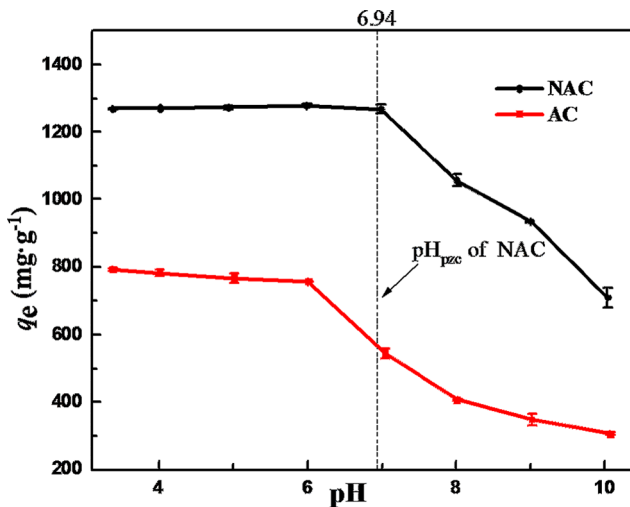## 3.3 The effect of dosage on adsorption of DOX

The dosage of activated carbons is an important parameter affecting the adsorption characteristics. As shown in Fig. 6(b), the NAC dosage increased from 0.05 g·L^{-1} to 0.25 g·L^{-1}, the removal efficiency of DOX increased from 39.09 to 99.48% and adsorption capacity per unit mass decreased from 1543.11 mg·g^{-1} to 802.18 mg·g^{-1}. On the one hand, the increase in the removal efficiency of DOX was due to the increase in the total specific surface area and availability of more adsorption sites with rising the NAC dosage. On the other hand, there was adsorption competition among NAC and a certain amount DOX molecule in liquid phase are evenly adsorbed onto more adsorbents, which leads to a decrease in adsorption capacity per unit mass. The AC had the similar adsorbed process as graph shown. Considering q_e and R %, 0.12 g·L^{-1} was selected to be the adsorbent dosage in subsequent adsorption experiments.

## 3.4 The effect of pH on adsorption of DOX

Solution pH influences adsorption process by changing the surface net charge of NAC and existing species of DOX. The curve of equilibrium adsorption capacity versus pH was displayed in Fig. 7. As initial solution pH increased from 3.38 to 6, the values of q_e for NAC had slight increasing from 1269.2 mg·g^{-1} to 1278.5 mg·g^{-1}. The adsorption capacity of NAC only had slight decreased when pH was within the range of 6–7, but decreased sharply under
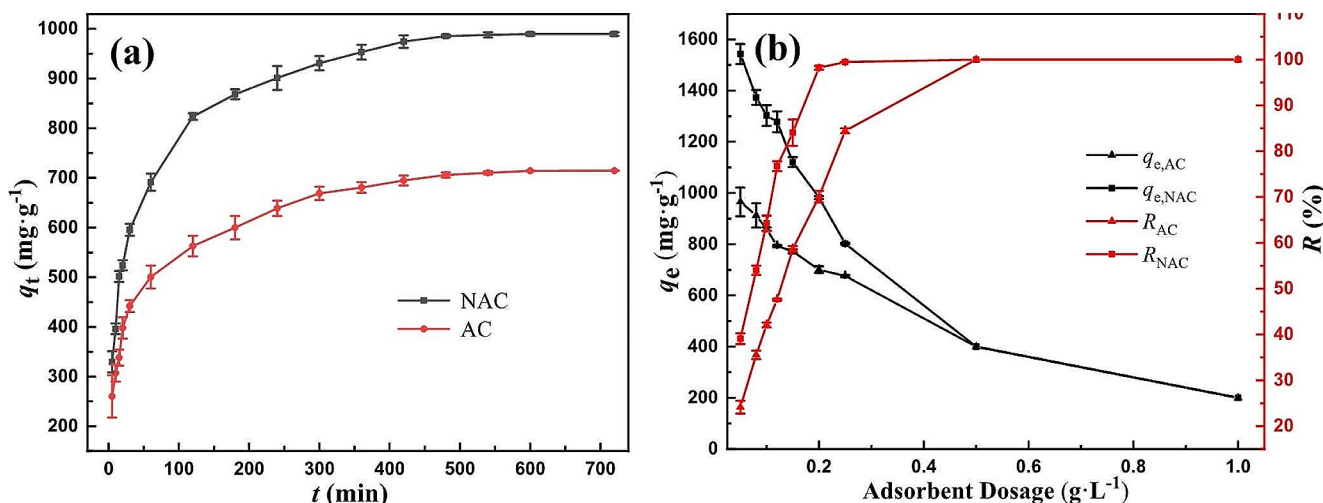
Fig. 6 Effect of time on the adsorption of DOX onto NAC and AC ($C_0 = 200$ mg·L^{-1}, adsorbents dosage = 0.2 g·L^{-1}, T = 298 K, pH = 3.38) **(a)** and effect of NAC and AC dosage on the adsorption of DOX ($C_0 = 200$ mg·L^{-1}, contact time = 540 min, T = 298 K, pH = 3.38) **(b)**

Fig. 7 Effect of pH on the adsorption of DOX ($C_0 = 200$ mg·L^{-1}, adsorbents dosage = 0.12 g·L^{-1}, contact time = 540 min, T = 298 K)
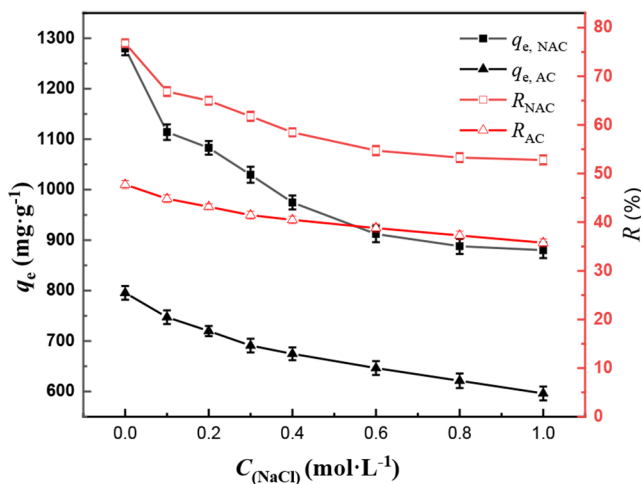
Fig. 8 Effect of salt ionic strength on the adsorption of DOX ($C_0 = 200$ mg L^{-1}; adsorbents dosage = 0.12 g·L^{-1}; contact time = 540 min, pH = 3.38, T = 298 K)
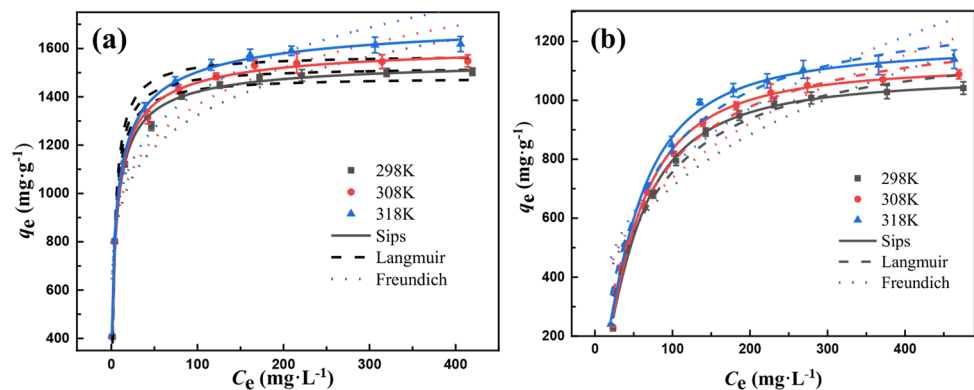
alkaline conditions. However, the adsorption capacity of AC always decreased from 793.50 mg·g^{-1} to 306.12 mg·g^{-1} with the increase of pH. Moreover, it can be observed that NAC could retain a relatively higher adsorption capacity for DOX in the larger pH range than AC. The probable reason was that the new formed the N-containing functional groups played a role in adsorption process. In addition, NAC demonstrated excellent adsorption capacity (1269.16 mg·g^{-1}) in the original solution of DOX. The pH of original DOX solution was near 3.38 and it was not adjusted in other experiments.

3.5 The effect of salt ionic on strength

The effect of salt ionic strength on adsorption for DOX was studied by 0–1 mol L^{-1} NaCl solution at 298 K. As shown in Fig. 8, with the concentration of NaCl solution increased from 0 to 1.0 mol L^{-1}, the adsorption capacities of NAC and AC for DOX decreased from 1269.12 mg·g^{-1} and 793.50 mg·g^{-1} to 879.97 mg·g^{-1} and 596.04 mg·g^{-1}, the R% decreased from 76.80% and 47.72–52.80% and 35.76%, respectively. This trend is because salt ionic occupied the active sites on the surface of activated carbon, resultng in competitive adsorption with DOX molecules in the solution. However, at high Na$^+$ concentrations, the removal efficiency of NAC exceeds 52.80%. Besides, the impact of salt ionic on the on the adsorption of NAC is greater than that of AC.

3.6 Adsorption isotherms of NAC and AC

The isothermal adsorption models such as Langmuir, Freundlich and Sips were used to analyze the adsorption equilibrium data. Figure 9 showed the adsorption isotherms of DOX onto NAC and AC, and the fitting parameters calculated according to equations (Eq. S1-S3) were listed in Table 2.

From the Fig. 9(a), the adsorption capacities of DOX on NAC increased with increasing temperature. The

Fig. 9 Nonlinear fitting of adsorption data of NAC **(a)** and AC **(b)** with isotherms models (adsorbents dosage = 0.12 g·L^{-1}, contact time = 540 min, pH = 3.38)

Table 2 Isotherm parameters of DOX adsorption onto NAC and AC

	Parameters	NAC			AC		
		298 K	308 K	318 K	298 K	308 K	318 K
Langmuir	q_m	1482.56	1524.00	1575.07	1230.47	1282.94	1347.65
	K_L	0.272	0.278	0.279	0.01598	0.01604	0.01626
	χ^2	18.66	19.85	28.89	59.30	64.76	50.67
	R^2	0.9790	0.9727	0.9526	0.9687	0.9693	0.9724
Freundlich	K_F	653.01	669.95	686.00	162.26	166.33	174.19
	1/n	0.1535	0.1547	0.1577	0.3198	0.3232	0.3245
	χ^2	56.11	57.09	46.88	263.90	279.00	310.63
	R^2	0.8638	0.8785	0.9042	0.8352	0.8396	0.8385
Sips	q_{ms}	1559.35	1635.61	1759.41	1080.05	1121.21	1183.05
	K_s	0.202	0.225	0. 233	0.0199	0.0202	0.0203
	M	0.74	0.68	0.59	1.52	1.50	1.49
	R^2	0.9913	0.9969	0.9990	0.9916	0.9927	0.9966
	χ^2	2.60	2.52	0.85	5.72	4.92	4.50

Table 3 Comparison of adsorption capacity of doxycycline with different adsorbents

Materials	Adsorption capacity ($mg \cdot g^{-1}$)	References
Magnetic cellulose nanocrystal (MCNC)	15.00	[48]
Iron loaded sludge biochar	128.98	[49]
Graphene-like layered molybdenum disulfide	556.00	[50]
Spent black tea leaves	36.81	[51]
Rice straw biochar	432.90	[52]
Pumpkin seed shell activated carbon	23.60	[7]
CoFe2O4/rice husk silica nanocomposite	835.47	[53]
NTiO2/NiSA-(Si-TETA)-Cu(II) nanocomposite	682.15	[54]
NAC	1559.35	This article
AC	1080.05	This article

Table 4 Thermodynamic parameters of NAC and AC

sample	$\Delta G°$ ($kJ \cdot mol^{-1}$)			$\Delta H°$ ($kJ \cdot mol^{-1}$)	$\Delta S°$ ($J \cdot mol^{-1}$)
	298 K	308 K	318 K		
NAC	-9.06	-10.07	-11.37	25.31	115.31
AC	-2.83	-3.24	-3.80	11.49	48.00

determination coefficients (R^2) of the Langmuir model were lower than 0.98 and the values of χ^2 (Eq. S4) were relatively higher at different temperatures, indicating Langmuir model was not suitable to describe the DOX adsorption process on NAC [45]. The K_L increasing with temperature increase were illustrated the adsorption was more efficient at higher temperature [27]. The Freundlich model was used to describe the adsorption process of multilayer adsorption on heterogeneous surface, which is an empirical assumption. The Freundlich model was also failed to describe the adsorption characteristics of DOX due to the lower R^2 values (<0.91) and the higher χ^2 values (>46.88).

The equation of Sips model was combined with Langmuir and Freundlich models [46]. It can simplify to Freundlich model at low concentrations, while it is given to Langmuir isotherm at high adsorbate concentrations [47]. In this study, 1/M is the larger than 1 which reflects a more heterogeneous system. As shown in Table 2, the R^2 values of the Sips model were higher than 0.99 and the χ^2 were lower

than 2.60, indicating that the equilibrium data of DOX was well described by Sips model. The sorption for DOX on the NAC was mainly on heterogeneous surface. The values of q_{ms} and K_s all increased with increasing temperature. The saturated adsorption capacities of NAC were 1559.35 $mg \cdot g^{-1}$, 1635.61 $mg \cdot g^{-1}$, and 1759.41 $mg \cdot g^{-1}$ at 298, 308 and 318 K, respectively.

Similarly, the isotherm fitting data (Table 2) of DOX adsorption on AC was more agree with Sips model due to higher R^2 values (> 0.99) and the lower χ^2 values (< 5.73). The saturated adsorption capacities of AC were 1080.05 $mg \cdot g^{-1}$ at 298 K, suggesting nitrogen doping significantly enhanced the adsorption ability of NAC for DOX. Table 3 presented the maximum adsorption capacity of DOX on various materials. Comparing with other materials, the NAC used in this study had a relatively higher adsorption capacity, which might be caused by its high SSA and abundant N, O-containing functional groups. The NAC could be considered as a potential adsorbent for the removal of antibiotic such as DOX from aqueous system.

3.7 Thermodynamic properties of NAC and AC

The values of $\Delta G°$, $\Delta H°$, and $\Delta S°$.were calculated by equations (Eq. S5-S7) and the results were showed in Table 4. The values of thermodynamic parameters of NAC and AC have the same trend, which could be speculated that the adsorption process of NAC and AC for DOX was spontaneous, endothermic and randomness-increasing. NAC displayed the superior thermodynamic properties and

Table 5 Kinetic parameters of DOX adsorption onto NAC

	Parameters	298 K	308 K	318 K
Pseudo-first-order	q_{e1}	1153.19	1182.25	1213.46
	k_1	0.061	0.063	0.064
	R^2	0.7434	0.7330	0.7440
Pseudo-second-order	q_{e2}	1227.61	1258.15	1290.54
	$k_2 \times 10^5$	6.51	6.59	6.66
	R^2	0.8513	0.8767	0.8999
Elovich	a	605.97	657.53	679.78
	b	0.00603	0.00592	0.00578
	R^2	0.9953	0.9955	0.9964
Intra-particle diffusion	k_{t1}	93.35	97.16	100.54
	C_1	290.23	301.50	304.98
	R	0.9921	0.9867	0.9999
	k_{t2}	30.39	30.89	31.49
	C_2	652.75	664.96	702.83
	R	0.9900	0.9922	0.9318
	k_{t3}	3.05	3.48	3.81
	C_3	1176.48	1230.76	1253.03
	R	0.9983	0.9949	0.9626

adsorption capacity compared to AC, which demonstrated N doping had a positive influence on the adsorption process.

3.8 Adsorption kinetic of NAC

Adsorption kinetics was used to understand the adsorption process better. In order to study the relationship between adsorption amount and contact time, the kinetic experimental data were fitted by pseudo-first-order, pseudo-second-order, Elovich and inter-particle diffusion kinetic models (Eq. S8-S10). The regression curves of kinetic models were showed in Fig. 10 and the parameters of kinetics models were presented in Table 5. In Fig. 9(a), the adsorption capacity of DOX increased rapidly within 150 min and then increased slowly within the range of 150–540 min. Finally, the adsorption process of DOX reached dynamic equilibrium at 540 min. The correlation coefficient R^2 of the Elovich model were all greater than 0.99, implying that the Elovich model fitted adsorption data for DOX well. Meanwhile, The Elovich model has commonly been seen as the semi-empirical equation which could describe adsorption

process on heterogeneous solids [55]. The rate constant a (mg·g^{-1}·min^{-1}) of Elovich model increased with the increase of temperature, indicating the adsorption process of DOX on NAC was endothermic, which was consistent with the thermodynamic results.

The experiment data was further fitted by intra-particle diffusion model (Eq. S11) in Fig. 10(b). From the plot, the adsorption process could divided into the three straight linear sections: (1) DOX molecules in the solution diffused to the boundary layer on the surface of NAC, (2) DOX molecules diffused from the boundary layer on the surface of NAC to the interior of particles, and (3) the adsorption process had been achieved the dynamic adsorption equilibrium. Moreover, all of the three curves did not pass through the origin, suggesting that DOX removal was controlled by multiple processes of the boundary diffusion and intra-particle diffusion [56].

3.9 Adsorption mechanism

The point of zero charge (pH$_{pzc}$) was determined in order to further explore the surface properties of activated carbons. In Fig. 11(a), the corresponding pH$_{pzc}$ of NAC was approximately 6.94, indicating that the NAC surface net charge was positive when pH<6.94 and the surface charge was negative at pH>6.94 [57]. Three pK$_a$ values of DOX were 3.5, 7.9 and 9.1 [50, 58, 59], the distribution curves and main molecular forms of DOX were exhibited in Fig. 11(b). At pH<2, the predominant form was the cationic species (DOX$^+$), which gradually decreased as the pH increased. At pH 3.5, the proportions of DOX$^+$ and DOX$^\pm$ were equal. It existed primarily as zwitterionic species (DOX$^\pm$) at pH values between 3.5 and 7.9. At pH>7.9, it presented mainly as anionic species (DOX$^-$ and DOX^{2-}) because tricarbonyl system and phenolic diketone moiety loss protons [60]. From the Fig. 7, the adsorption capacity of DOX increased slightly from 1269.2 mg·g^{-1} to 1278.5 mg·g^{-1} with pH increased from 3.38 to 6. Nevertheless, the adsorption capacity of DOX gradually reduced to 1268.0 mg·g^{-1} within the pH range of 6–7, but the adsorption capacity decreased sharply at pH>7.

Fig. 10 Nonlinear fitting of adsorption data with the kinetic models of pseudo first-order, pseudo second-order, Elovich (a) and intra-particle diffusion model (C_0=200 mg·L^{-1}, adsorbents dosage=0.12 g·L^{-1}, pH=3.38) (b)
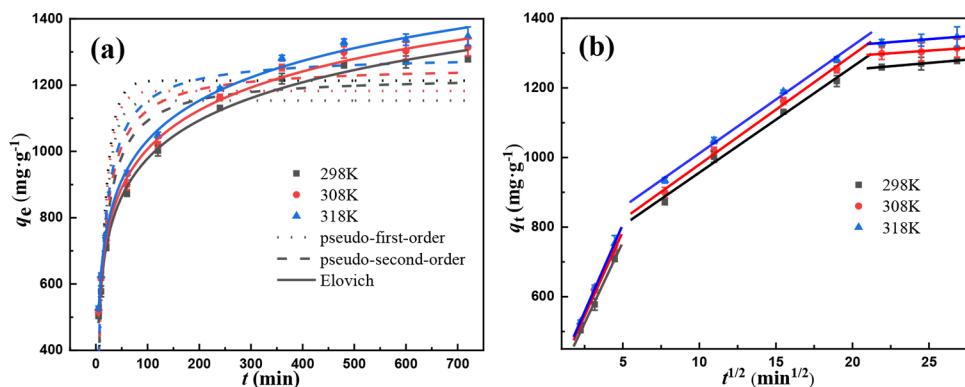
NAC manifested a high adsorption capacity for DOX, and it was supposedly ascribed to the hydrogen bonding and π-π electron donor-acceptor (EDA) interaction between the NAC and DOX. FTIR revealed that substantial number of hydroxyl and carbonyl groups were on NAC, which could participate in the formation of hydrogen bonds to promote adsorption [61]. DOX adsorption occurred mainly via H-bonds between the C=O of the NAC and the -OH or N-H groups of DOX as well as via bonding between C=O of DOX and the -OH or N-H of NAC. As discussed above in the XPS analysis of the NAC, the binding energy shift of C=O and C-O-H also indicates that the adsorption of DOX is partly through the hydrogen bonds between the NAC and DOX. The Raman spectrum suggested the existence of numerous of aromatic rings related with electron deficiency on NAC, which could serve as π-electron acceptors [43]. Besides, the graphitic-N in NAC could function as a π-acceptor owing to the high electronegativity of N. Therefore, the DOX as π-donors could be adsorbed on NAC via the π-π EDA interaction.

According to studies on pH, electrostatic interaction and hydrophobic interaction also be taken into consideration in the DOX adsorption. At pH 3.38-4, the q_e increased slightly because the decrease in quantities of DOX$^+$ led to weaken a part of electrostatic repulsion force between the positive charge of NAC and DOX$^+$. Meanwhile, as pH increased from 4 to 6, the values of q_e had a slight increase with the increase of pH, which is mainly attributed to the hydrophobic interactions. At pH 6–7, a slight decrease of q_e due to the hydrophobic interactions weakened. When pH > 7, the electrostatic repulsion force between the negative charge of NAC and DOX$^-$/DOX^{2-} was gradually increased, which limited the adsorption for DOX. Meanwhile, the adsorption capacity of NAC decreases with pH increasing, which might be due to the reduction of hydrogen bond because of DOX ionization [62, 63].

The graphical illustration of adsorption mechanism of DOX onto NAC was shown in Fig. 11(c). In summary, the adsorption of DOX onto NAC could be achieved through the H-bonding, π-π EDA interaction, hydrophobic interaction and electrostatic interaction.
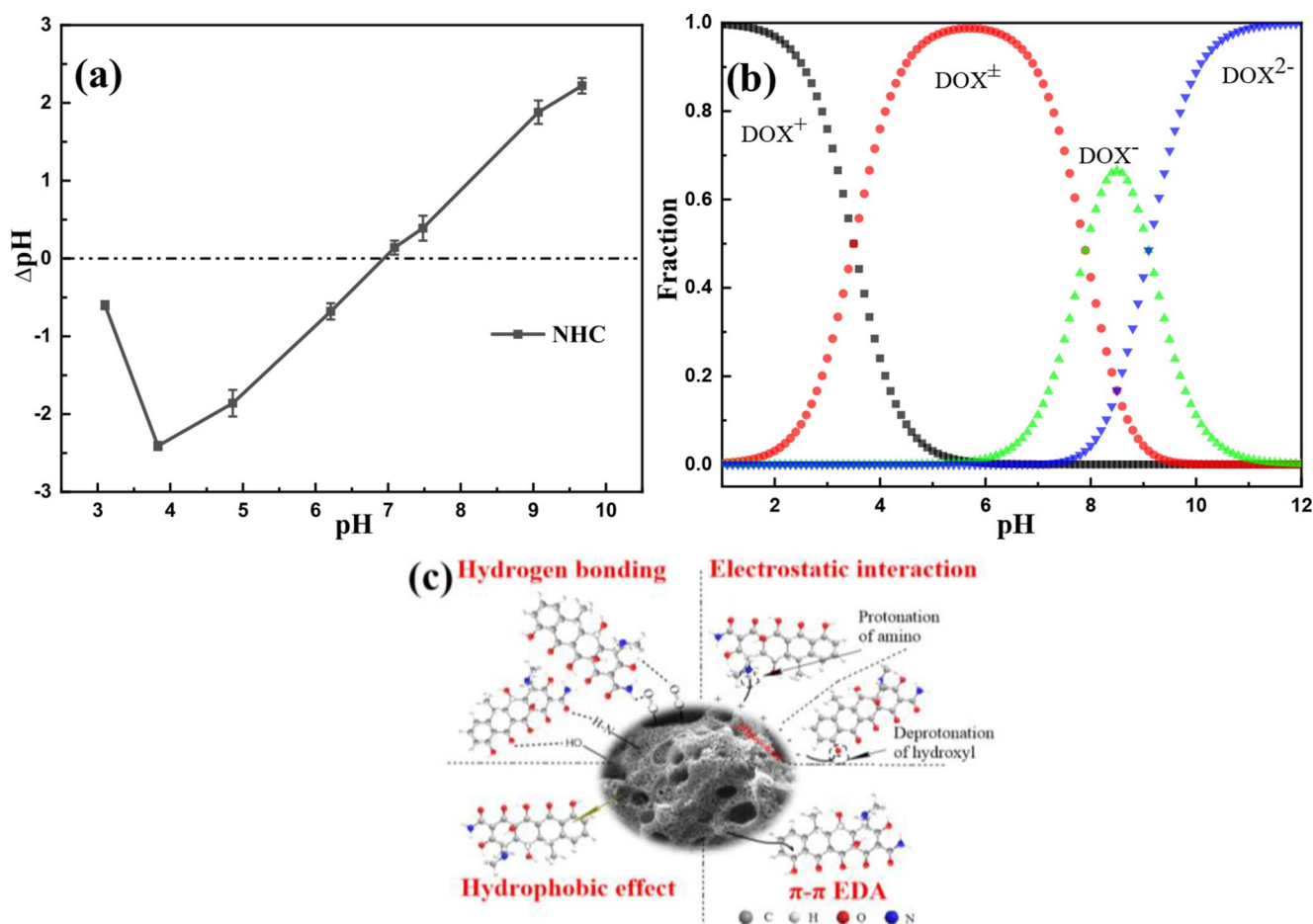
Fig. 11 The point of zero charge (pHpzc) of NAC **(a)**, existing species forms of DOX at different pH **(b)**, graphical illustration of adsorption mechanism of NAC **(c)**
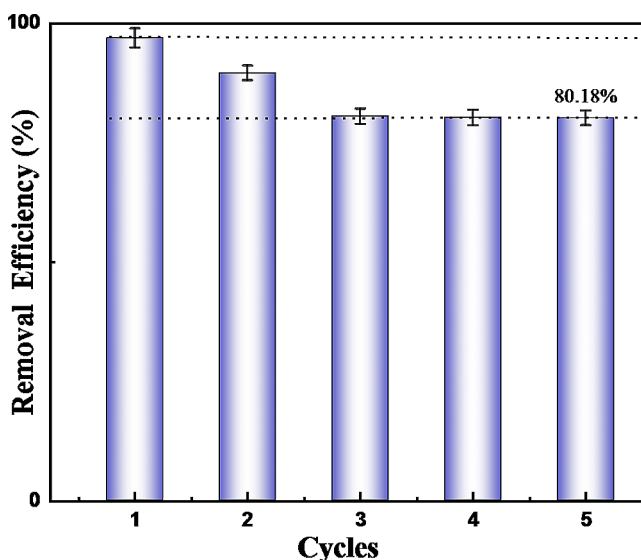
Fig. 12 Recyclability of NAC for the adsorption of DOX ($C_0 = 200$ mg·L^{-1}, adsorbent dosage $= 0.2$ g·L^{-1}, $C_0 = 200$ mg·L^{-1}, T $= 298$ K, pH $= 3.38$)

3.10 Regeneration adsorption experiment

Reusability of is an essential sector to evaluate the usage life of NAC. The regeneration adsorption experiments were carried out by the DOX solution (200 mg·L^{-1}) at 298 K. It should be emphasized that the removal efficiency only displayed a slight decrease to 90.0% on the second cycle, and it remained at approximately 80.0% even after 5 consecutive cycles as shown in Fig. 12. This clearly indicated that the NAC demonstrated an excellent regeneration ability and satisfactory recovery for DOX.

4 Conclusions

In this study, the N-doped activated carbon was prepared from agricultural waste pomelo peel. The adsorption experiments for the removal of DOX showed that the NAC had better adsorptive performance than AC. The testing adsorption data of NAC better fitted Sips isotherm model and Elovich kinetic model model. The maximum saturated adsorption capacities of NHC were 1559.35 mg·g^{-1} at 298 K. Characterizations showed NAC had more well-developed pore structure, defects and N content than AC, which indicated using melamine as an external nitrogen source, through hydrothermal carbonization, nitrogen doping, and activation is a good way to prepare high specific surface area N-doped activated carbon. Moreover, the nitrogen-doped could provide more adsorption sites and N-containing functional groups, which strengthened the adsorption capacity of NAC for DOX. Overall, the NAC prepared from a low cost

agricultural waste was a promising adsorbent for application in the control of antibiotics pollution, which has important practical guidance significance in the field of wastewater treatment.

Data availability No datasets were generated or analysed during the current study.

Declarations

References

1. S.M. Zainab, M. Junaid, N. Xu, R.N. Malik, Antibiotics and antibiotic resistant genes (ARGs) in groundwater: a global review on dissemination, sources, interactions, environmental and human health risks. Water Res. **187**, 116455 (2020). https://doi.org/10.1016/j.watres.2020.116455

2. L. Du, S. Ahmad, L. Liu, L. Wang, J. Tang, A review of antibiotics and antibiotic resistance genes (ARGs) adsorption by biochar and modified biochar in water. Sci. Total Environ. **858**(2), 159815 (2023). https://doi.org/10.1016/j.scitotenv.2022.159815

3. C. Teodosiu, A.-F. Gilca, G. Barjoveanu, S. Fiore, Emerging pollutants removal through advanced drinking water treatment: a review on processes and environmental performances assessment. J. Clean. Prod. **197**(1), 1210–1221 (2018). https://doi.org/10.1016/j.jclepro.2018.06.247

4. N. Stambouli, A. Driss, F. Gargouri et al., COVID-19 prophylaxis with doxycycline and zinc in health care workers: a prospective, randomized, double-blind clinical trial. Int. J. Infect. Dis. **122**, 553–558 (2022). https://doi.org/10.1016/j.ijid.2022.06.016

5. M.S. Gaballah, J. Guo, H. Sun et al., A review targeting veterinary antibiotics removal from livestock manure management systems and future outlook. Bioresour Technol. **333**, 125069 (2021). https://doi.org/10.1016/j.biortech.2021.125069

6. X. Yang, Y. Li, F. Kong, X. Sun, S. Wang, Y. Cui, Effect of ZnFe-LDHs modified oyster shell on the removal of tetracyclines antibiotics and variation of tet genes in vertical flow constructed wetlands. Chem. Eng. J. **431**(3), 134093 (2022). https://doi.org/10.1016/j.cej.2021.134093

7. G. Kaur, N. Singh, A. Rajor, Adsorption of doxycycline hydrochloride onto powdered activated carbon synthesized from pumpkin seed shell by microwave-assisted pyrolysis. Environ.

Technol. Inno. **23**, 101601 (2021). https://doi.org/10.1016/j.eti.2021.101601

8. S. Bahmanzadeh, M. Noroozifar, Fabrication of modified carbon paste electrodes with Ni-doped Lewatit FO_{36} nano ion exchange resin for simultaneous determination of epinephrine, Paracetamol and tryptophan. J. Electroanal. Chem. **809**, 153–162 (2018). https://doi.org/10.1016/j.jelechem.2017.11.073

9. D. Fu, T.A. Kurniawan, H. Li, L. Wang et al., Applicability of HDPC-supported Cu nanoparticles composite synthesized from anaerobically digested wheat straw for octocrylene degradation in aqueous solutions. Chem. Eng. J. **355**, 650–660 (2019). https://doi.org/10.1016/j.cej.2018.08.188

10. M. Yuan, C. Li, B. Zhang, J. Wang, J. Zhu, J. Ji, Y. Ma, A mild and one-pot method to activate lignin-derived biomass by using boric acid for aqueous tetracycline antibiotics removal in water. Chemosphere. **280**, 130877 (2021). https://doi.org/10.1016/j.chemosphere.2021.130877

11. Y. Li, H. Yu, L. Liu, H. Yu, Application of co-pyrolysis biochar for the adsorption and immobilization of heavy metals in contaminated environmental substrates. J. Hazard. Mater. **420**, 126655 (2021). https://doi.org/10.1016/j.jhazmat.2021.126655

12. A. Ejsmont, J. Goscianska, Morphology controlled nitrogen-doped mesoporous carbon vehicles for sustained release of Paracetamol. Micropor Mesopor Mater. **350**, 112449 (2023). https://doi.org/10.1016/j.micromeso.2023.112449

13. X. Zhou, S. Liu, Y. Hu, J. He, W. Zhang, R. Hong et al., Green synthesis of porous bamboo-based activated carbon with high VOCs adsorption performance via steam activation method. J. Porous Mater. **31**, 737–746 (2024). https://doi.org/10.1007/s10934-024-01557-0

14. D. Fu, T.A. Kurniawan, H. Gui et al., Role of Cu_xO-Anchored Pyrolyzed hydrochars on H_2O_2-Activated degradation of tetracycline: effects of Pyrolysis temperature and pH. Ind. Eng. Chem. Res. **61**(25), 8847–8857 (2022). https://doi.org/10.1021/acs.iecr.2c01100

15. A. Tomczyk, B. Kondracki, K. Szewczuk-Karpisz, Chemical modification of biochars as a method to improve its surface properties and efficiency in removing xenobiotics from aqueous media. Chemosphere. **312**(1), 137238 (2023). https://doi.org/10.1016/j.chemosphere.2022.137238

16. M.S. Md Zaini, S.A.M. Al-Junid, S.S.A. Syed-Hassan, Effects of nitrogen doping on lithium polysulfide anchoring by activated carbon derived from palm kernel shell. J. Porous Mater. (2024). https://doi.org/10.1007/s10934-024-01556-1

17. N. Kasera,, P. Kolar, S.G. Hall, Nitrogen-doped biochars as adsorbents for mitigation of heavy metals and organics from water: a review. Biochar. **4**, 17 (2022). https://doi.org/10.1007/s42773-022-00145-2

18. M. Yue, X. Jiang, S. Zhang, Y. Li, W. Xu, N-doped carbons accelerate the reducing decomposition of copper nitrate and construct bifunctional adsorbents for adsorption desulfurization. Micropor Mesopor Mater. **282**, 100–108 (2019). https://doi.org/10.1016/j.micromeso.2019.03.026

19. Y. Fan, Z. Zhao, Q. Zhou, G. Li, X. Wang, J. Qiu, Y. Gogotsi, Nitrogen-doped carbon microfibers with porous textures. Carbon. **58**, 128–133 (2013). https://doi.org/10.1016/j.carbon.2013.02.040

20. S. Lang, S. Zhang, Z. Cao, J. Yang, Y. Zhou, S. Liu, J. Xu, C. Yang, Improvement of hydrochar/biochar pellets prepared from cotton stalk by hydrothermal pretreatment process. J. Anal. Appl. Pyrol. **176**, 106263 (2023). https://doi.org/10.1016/j.jaap.2023.106263

21. A.H. Gedam, R.S. Dongre, Comparative study of sponge gourd derived biochar and activated carbon for bio-sorption and desorption of Pb(II) ions, Mater. Today: Proceedings, 18(3), 887–900 (2019). https://doi.org/10.1016/j.matpr.2019.06.521

22. Y. Wu, X. Fang, X. Shen, X. Yu, C. Xia, L. Xu, Y. Zhang, L. Gan, Synergetic effect of photocatalytic oxidation plus catalytic oxidation on the performance of coconut shell fiber biochar decorated α-MnO_2 under visible light towards BPA degradation. J. Environ. Manage. **345**, 118911 (2023). https://doi.org/10.1016/j.jenvman.2023.118911

23. Y. Wei, S. Fakudze., Y. Zhang, R. Ma, Q. Shang, J. Chen, C. Liu, Q. Chu, Co-hydrothermal carbonization of pomelo peel and PVC for production of activated carbon pellets with enhanced fuel properties and dechlorination. Energy. **239**, 122350 (2022). https://doi.org/10.1016/j.energy.2021.122350

24. Asadullah, L. Kaewsichan, K. Tohdee. Adsorption of hexavalent chromium onto alkali-modified biochar derived from Lepironia articulata: a kinetic, equilibrium, and thermodynamic study. Water Environ. Res. **91**(11), 1433–1446 (2019). https://doi.org/10.1002/wer.1138

25. R. Slimani, I. El Ouahabi, F. Abidi, M. El Haddad et al., Calcined eggshells as a new biosorbent to remove basic dye from aqueous solutions: thermodynamics, kinetics, isotherms and error analysis. J. Taiwan. Inst. Chem. E. **45**, 1578–1587 (2014). https://doi.org/10.1016/j.jtice.2013.10.009

26. Y. He, Z. Guo, M. Chen et al., Efficient adsorption of methyl orange and methylene blue dyes by a novel carbazole-based hyper-crosslinked porous polymer. J. Porous Mater. **30**, 1439–1448 (2023). https://doi.org/10.1007/s10934-023-01434-2

27. H. Guo, S. Cheng, B. Xing., M. Meng, L. Feng, Y. Nie, C. Zhang, Preparation of three kinds of efficient sludge-derived adsorbents for metal ions and organic wastewater purification. Arab. J. Chem. **17**(4), 105671 (2024). https://doi.org/10.1016/j.arabjc.2024.105671

28. Y. Wang, L. Chen, C. Chen, J. Xi et al., Occurrence of both hydroxyl radical and surface oxidation pathways in N-doped layered nanocarbons for aqueous catalytic ozonation. Appl. Catal. B- Environ. **254**, 283–291 (2019). https://doi.org/10.1016/j.apcatb.2019.05.008

29. S. Naeimi, H. Faghihian, Application of novel metal organic framework, MIL-53(Fe) and its magnetic hybrid: for removal of pharmaceutical pollutant, doxycycline from aqueous solutions. Environ. Toxicol. Pharmacol. **53**, 121–132 (2017). https://doi.org/10.1016/j.etap.2017.05.007

30. S. Liu, W. Xu, Y. Liu, X. Tan, G. Zeng et al., Facile synthesis of Cu(II) impregnated biochar with enhanced adsorption activity for the removal of doxycycline hydrochloride from water. Sci. Total Environ. **592**, 546–553(2017), https://doi.org/10.1016/j.scitotenv.2017.03.087

31. F.-C. Huang, C.-K. Lee, Y.-L. Han, W.-C. Chao, H.-P. Chao, Preparation of activated carbon using micro-nano carbon spheres through chemical activation. J. Taiwan. Inst. Chem. E. **45**(5), 2805–2812 (2014). https://doi.org/10.1016/j.jtice.2014.08.004

32. B. Li, J. Guo, K. Lv, J. Fan, Adsorption of methylene blue and Cd(II) onto maleylated modified activated carbon from water. Environ. Pollut. **254**, 113014 (2019). https://doi.org/10.1016/j.envpol.2019.113014

33. K.C. Bedin, A.L. Cazetta, I.P.A.F. Souza et al. Porosity enhancement of spherical activated carbon: influence and optimization of hydrothermal synthesis conditions using response surface methodology. J. Environ. Chem. Eng. **6**(1), 991–999 (2018). https://doi.org/10.1016/j.jece.2017.12.069

34. J.L. Liu, W.C. Qian, J.Z. Guo, Y. Shen, B. Li, Selective removal of anionic and cationic dyes by magnetic Fe_3O_4-loaded amine-modified activated carbon. Bioresour Technol. **320**, 124374 (2021). https://doi.org/10.1016/j.biortech.2020.124374

35. X. Qin, S. Cheng, B. Xing et al., Preparation of pyrolysis products by catalytic pyrolysis of poplar: application of biochar in antibiotic wastewater treatment. Chemosphere. **338**, 139519 (2023). https://doi.org/10.1016/j.chemosphere.2023.139519

36. H. Wang, W. Guo, B. Liu., Q. Wu et al., Edge-nitrogenated biochar for efficient peroxydisulfate activation: an electron

transfer mechanism. Water Res. **160**, 405–414 (2019). https://doi.org/10.1016/j.watres.2019.05.059

37. Y. Chen, G. Zhang, J. Zhang, H. Guo et al., Synthesis of porous carbon spheres derived from lignin through a facile method for high performance supercapacitors. J. Mater. Sci. Technol. **34**, 2189–2196 (2018). https://doi.org/10.1016/j.jmst.2018.03.010

38. L. Deng, B. Lu, J. Li et al., Effect of pore structure and oxygen-containing groups on adsorption of dibenzothiophene over activated carbon. Fuel. **200**, 54–61 (2017). https://doi.org/10.1016/j.fuel.2017.03.018

39. M. Ayiania, M. Smith, A.J.R. Hensley et al., Deconvoluting the XPS spectra for nitrogen-doped chars: an analysis from first principles. Carbon. **162**, 528–544 (2020). https://doi.org/10.1016/j.carbon.2020.02.065

40. C. Zheng, Z. Yang, M. Si et al., Application of biochars in the remediation of chromium contamination: fabrication, mechanisms, and interfering species. J. Hazard. Mater. **407**, 124376 (2021). https://doi.org/10.1016/j.jhazmat.2020.124376

41. H. Shang, Y. Li, J. Liu et al., Preparation of nitrogen doped magnesium oxide modified biochar and its sorption efficiency of lead ions in aqueous solution. Bioresour Technol. **314**, 123708 (2020). https://doi.org/10.1016/j.biortech.2020.123708

42. N. Liu, Y. Zhang, C. Xu et al., Removal mechanisms of aqueous cr(VI) using apple wood biochar: a spectroscopic study. J. Hazard. Mater. **384**, 121371 (2020). https://doi.org/10.1016/j.jhazmat.2019.121371

43. D.R. Lima, A. Hosseini-Bandegharaei, Efficient acetaminophen removal from water and hospital effluents treatment by activated carbons derived from Brazil nutshells. Colloids Surf. A **583** (2019). https://doi.org/10.1016/j.colsurfa.2019.123966

44. B. Li., Q. Wang, J.-Z. Guo, W.-W. Huan, L. Liu, Sorption of methyl orange from aqueous solution by protonated amine modified activated carbon. Bioresour Technol. **268**, 454–459 (2018). https://doi.org/10.1016/j.biortech.2018.08.023

45. S. Cheng, S. Zhao., B. Xing, C. Shi et al., Facile one-pot green synthesis of magnetic separation photocatalyst-adsorbent and its application. J. Water Process. Eng. **47**, 102802 (2022). https://doi.org/10.1016/j.jwpe.2022.102802

46. R. Saadi, Z. Saadi, R. Fazaeli, N.E. Fard, Monolayer and multilayer adsorption isotherm models for sorption from aqueous media. Korean J. Chem. Eng. **32**, 787–799 (2015). https://doi.org/10.1007/s11814-015-0053-7

47. D.S. Tong, C.W. Wu, M.O. Adebajo et al., Adsorption of methylene blue from aqueous solution onto porous cellulose-derived carbon/montmorillonite nanocomposites. Appl. Clay Sci. **161**, 256–264 (2018). https://doi.org/10.1016/j.clay.2018.02.017

48. A.I.A. Soliman, J.A. Díaz Baca, P. Fatehi, One-pot synthesis of magnetic cellulose nanocrystal and its post-functionalization for doxycycline adsorption. Carbohydr. Polym. **308**, 120619 (2023). https://doi.org/10.1016/j.carbpol.2023.120619

49. Y. Chao, W. Zhu, Application of graphene-like layered molybdenum disulfide and its excellent adsorption behavior for doxycycline antibiotic. Chem. Eng. J. **243**, 60–67 (2014). https://doi.org/10.1016/j.cej.2013.12.048

50. J. Wei, Y. Liu, J. Li, Y. Zhu, H. Yu, Y. Peng, Adsorption and co-adsorption of tetracycline and doxycycline by one-step synthesized iron loaded sludge biochar. Chemosphere. **236**, 124254 (2019). https://doi.org/10.1016/j.chemosphere.2019.06.224

51. L. Xing, K.M. Haddao, N. Emami et al., Fabrication of HKUST-1/ZnO/SA nanocomposite for doxycycline and Naproxen adsorption from contaminated water. Sustain. Chem. Pharm. **29**, 100757 (2022). https://doi.org/10.1016/j.scp.2022.100757

52. Z.W. Zeng, X.F. Tan, Y.G. Liu et al., Comprehensive adsorption studies of doxycycline and ciprofloxacin antibiotics by biochars prepared at different temperatures. Front. Chem. 6, (MAR) (2018). https://doi.org/10.3389/fchem.2018.00080

53. S.J. Olusegun, N.D.S. Mohallem, Insight into the adsorption of doxycycline hydrochloride on different thermally treated hierarchical $CoFe_2O_4$/bio-silica nanocomposite. J. Environ. Chem. Eng. **7**, 103442 (2019). https://doi.org/10.1016/j.jece.2019.103442

54. M.E. Mahmoud, M.F. Amira, S.M. Seleim, A.K. Mohamed, Insight into the adsorption of doxycycline hydrochloride on different thermally treated hierarchical $CoFe_2O_4$/bio-silica nanocomposite. J. Chem. Eng. Data. **65**, 3546–3559 (2020). https://doi.org/10.1021/acs.jced.0c00112

55. N.Y. Mezenner, A. Bensmaili, Kinetics and thermodynamic study of phosphate adsorption on iron hydroxide-eggshell waste. Chem. Eng. J. **147**, 87–96 (2009). https://doi.org/10.1016/j.cej.2008.06.024

56. J. Wang, X. Guo, Adsorption kinetic models: physical meanings, applications, and solving methods. J. Hazard. Mater. **390**, 122156 (2020). https://doi.org/10.1016/j.jhazmat.2020.122156

57. D. Fu, T.A. Kurniawan, Y. Wang, Z. Zhou, Q. Wei, Y. Hu, H. Dzarfan Othman, M. Wayne Chew, K. Hwang Goh, H. Gui, Applicability of magnetic biochar derived from Fe-enriched sewage sludge for chromate removal from aqueous solution. Chem. Eng. Sci. **281** (2023). https://doi.org/10.1016/j.ces.2023.119145

58. Y. Zhang, F.Q. Jiang, D.Y. Huang et al., A facile route to magnetic mesoporous core-shell structured silicas containing covalently bound cyclodextrins for the removal of the antibiotic doxycycline from water. Rsc Adv. **8**, 31348–31357 (2018). https://doi.org/10.1039/c8ra05781h

59. C.O. Aniagor, C.A. Igwegbe, J.O. Ighalo, S.N. Oba, Adsorption of doxycycline from aqueous media: a review. J. Mol. Liq. **334** (2021). https://doi.org/10.1016/j.molliq.2021.116124

60. S.J. Liu, Y.G. Liu, X.F. Tan et al., Facile synthesis of MnO_X-loaded biochar for the removal of doxycycline hydrochloride: effects of ambient conditions and co-existing heavy metals. J. Chem. Technol. Biotechnol. **94**, 2187–2197 (2019). https://doi.org/10.1002/jctb.6000

61. L. Zhou, Y.F. Huang, W.W. Qiu et al., Adsorption properties of Nano-MnO_2-Biochar composites for copper in aqueous solution. Molecules. **22**(1), 173 (2017). https://doi.org/10.3390/molecules22010173

62. I. Villaescusa, N. Fiol, J. Poch, A. Bianchi, C. Bazzicalupi, Mechanism of Paracetamol removal by vegetable wastes: the contribution of π–π interactions, hydrogen bonding and hydrophobic effect. Desalination. **270**, 135–142 (2011). https://doi.org/10.1016/j.desal.2010.11.037

63. D.D. Sewu, H. Jung, S.S. Kim et al., Decolorization of cationic and anionic dye-laden wastewater by steam-activated biochar produced at an industrial-scale from spent mushroom substrate. Bioresoure Technol. **277**, 77–86 (2019). https://doi.org/10.1016/j.biortech.2019.01.034